J Mater Sci (2016) 51:8296–8309

Amine-graphene oxide/waterborne polyurethane nanocomposites: effects of different amine modifiers on physical properties

Ling Hu[1], Pingping Jiang[1,*], Pingbo Zhang[1], Gang Bian[1], Songsong Sheng[1], Min Huang[1], Yanmin Bao[2], and Jialiang Xia[2]

[1] *The Key Laboratory of Food Colloids and Biotechnology, School of Chemical and Material Engineering, Jiangnan University, Wuxi 214122, People's Republic of China*

[2] *Jiangsu Caihua Packaging Group Company, Kunshan 215321, People's Republic of China*

Received: 28 January 2016
Accepted: 15 April 2016
Published online: 16 June 2016

ABSTRACT

To study the dispersity of different amine-graphene oxide (amine-GO) in polymer matrix and the interfacial interactions between functionalized graphene oxide and matrix, two kinds of modifiers—organoamine- and aminosilane-coupling agents—were used to functionalize graphene nanosheets to obtain functionalized graphene oxide/waterborne polyurethane nanocomposites by in situ polymerization. The chemical structure, morphology, and interlayer space of amine-GO nanoplatelets were confirmed by FT-IR, Raman, TGA, XPS, TEM, AFM, and XRD. The dispersity behaviors between different amine-GOs and polymers were evaluated by FESEM. The thermal, mechanical, and hydrophobic properties of the nanocomposites were investigated by TGA, tensile testing machine, and water contact angle test, respectively. It was found that the tensile strength of nanocomposites was increased from 10.13 to 27.79 and 28.96 Mpa after the addition of amine-GO functionalized by APTMS and APTES, respectively. The better thermal stability and hydrophobicity of nanocomposites were also achieved by the addition of amine-GO, especially those modified by aminosilane-coupling agents. This study paves a new route for designing and developing chemically converted graphene oxide nanosheets/polymer nanocomposite materials by altering suitable amine-modifier to functionalize graphene oxide nanosheets and then optimizing the interphases between graphene oxide nanosheets and polymer matrices.

Address correspondence to E-mail: ppjiang@jiangnan.edu.cn

DOI 10.1007/s10853-016-9993-5

Introduction

Waterborne polyurethane (WPU), a better versatile environmentally friendly material, is one kind of flexible and elastic polymer mainly synthesized by the reaction of diisocyanates with diols, as shown in Scheme 1i, and is widely used in coatings, adhesives, sealants, and thermoplastic elastomers [1]. However, some inferior properties of waterborne polyurethanes, such as low mechanical strength and water resistance, have limited its available application range, and hence, problems related to their properties and processing can largely be resolved by proper molecular designs and hybridization with other materials [2–7].

Hybrid organic–inorganic nanostructure composites based on polymer matrix and inorganic matter have attracted great interest of researchers because they exhibit the enhanced performance properties compared with conventional composites owing to the maximized interfacial contact between the organic and inorganic phases [8–10]. Graphene, as a novel inorganic material, attracts more interest in the area of polymer composites during the past few years owing to excellent characteristics such as high mechanical properties (approximately 1000 GPa) [11, 12], excellent electrical conductivity (approximately 6000 S cm^{-1}) [13], thermal conductivity (approximately 5000 Wm^{-1} K^{-1}) [14], high surface area (2630 m^2 g^{-1}) [15], and gas impermeability [16]; this implies that graphene as reinforcing agents may improve the drawback of WPU. In general, graphene-based WPU composites are fabricated by solution-processable blending nanofillers into polymer matrix [5, 10, 17]. Unfortunately, the homogeneous dispersion and efficient interfacial interactions are still the main challenges for this method due to the strong tendency to aggregation of the graphene nanosheets (GNSs). In this respect, it is imperative to develop a facile and friendly method to efficiently vest graphene with high dispersity in solvents or polymer matrix with the assistance of simultaneous surface modification. Covalent functionalization on the surface of GNSs is an effective strategy for fabricating GNS-based polymer composites, which is an available method for improving the interfacial interactions between GNSs and polymer matrix [18–23]. The graphene oxide (GO), the precursor of GNS, has abundant functional groups on the surface including hydroxyls, epoxides, and carboxyls, which provide the reactive site for covalent functionalization. Moreover, the covalent functionalization significantly alters the Van der Waals interactions among the nanofiller aggregates, making them easy to be dispersed in the polymer matrix [24, 25].

In this work, the interfacial interactions between different amine-GO nanosheets and WPU chains have been investigated in-depth. Afterward, we compared the effects of different amine-GO nanosheets on the properties of nanocomposites. According to the obtained results, an efficient dispersion of amine-GO nanosheets in WPU, and covalent bonding with PU chains were achieved via a better modifier to functionalize graphene. More specifically, waterborne polyurethane nanocomposites reinforced with two kinds of amine-GO modified by organoamine- and aminosilane-coupling agents were prepared by in situ polymerization, respectively, as shown in Scheme 1ii, in which ethylenediamine (EDA) and triethylenetetramine (TETA) were used as the organoamine; likewise, 3-aminopropyltriethoxysilane (APTES) and 3-aminopropyltrimethoxysilane (APTMS) were chosen as the second modifier. Thus, we attempted to react $–NH_2$ featured on the surface of functionalized graphene sheets with –NCO of PU chains by in situ polymerization. In this way, a well-dispersed nanocomposite was fabricated after considering the existence of hydrogen bonds, such as the interactions between the remaining oxygen left on the nanosheets and urethane linkages. Based on the above mechanism, therefore, the effects of different amine-GO nanosheets on the physical properties including thermal properties, mechanical properties, and hydrophobicity of nanocomposite were investigated.

Experiment

Synthesis of graphene oxide

Graphene oxide was prepared from graphite (44-mm average particle diameter, Qingdao Jinrilai Graphite Co. Ltd., Qingdao, China) by traditional Hummers' method with a little change as reported elsewhere [26]. In brief, 2 g of graphite and 1 g of $NaNO_3$ were added to a 500 mL three-necked flask. The flask was put on an ice bath to control the temperature, 100 mL of concentrated H_2SO_4 was slowly added to the flask. Then, 6 g of $KMnO_4$ was slowly added with vigorous stirring for 2 h. The flask was then taken off the ice

Scheme 1 (**i**) Preparation procedure of synthesizing the WPU emulsion. (**ii**) Illustration of the fabrication of amine-GO/WPU nanocomposites.

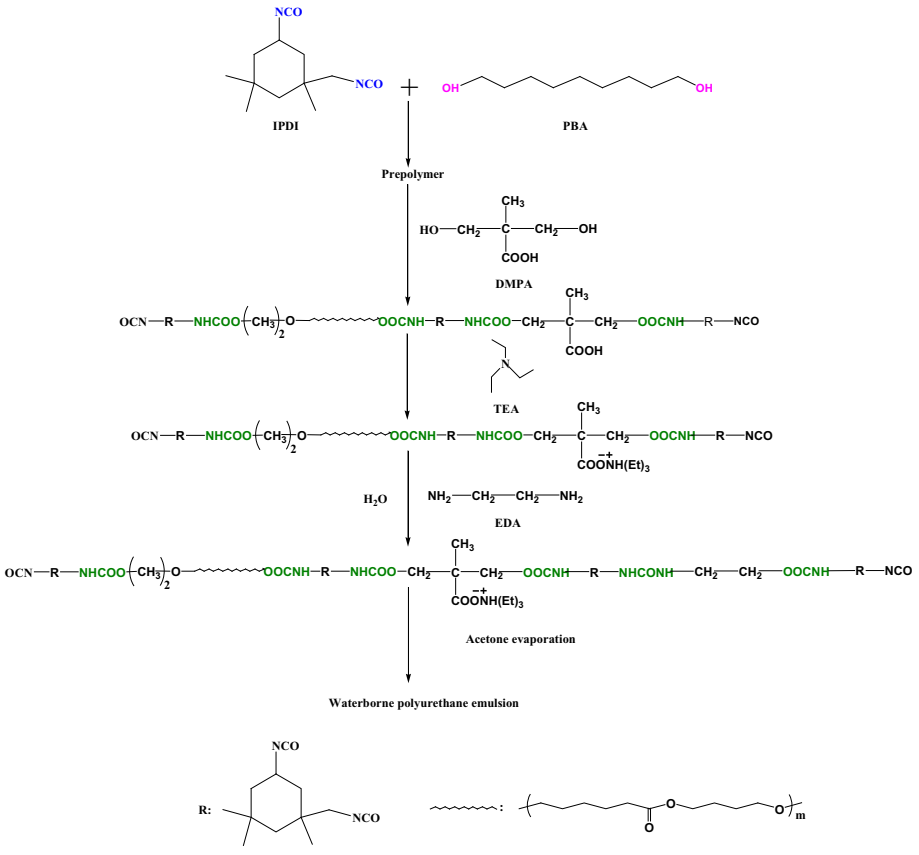

i

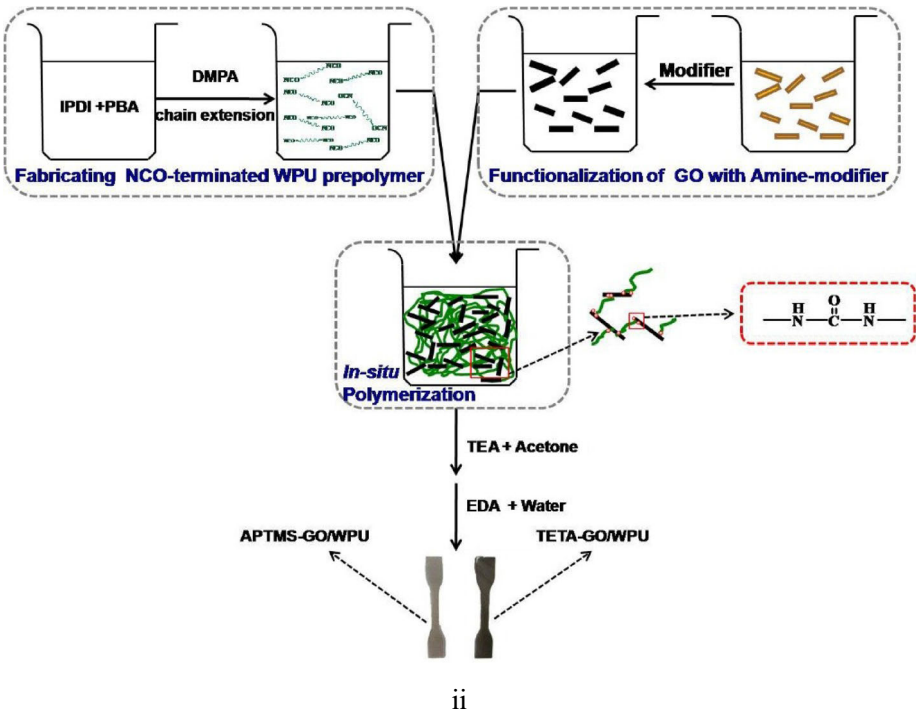

ii

bath and kept at room temperature for several days (3–6 days). 5 wt% H_2SO_4 aqueous solution (175 mL) was used to dilute the mixture over 1 h, and then stirred for another 2 h at 98 °C. After the solution cooled to 60 °C, 30 wt% H_2O_2 (7.5 mL) was added, and the mixture was stirred for 2 h again. The resultant yellowish-brown mixture was then centrifuged (6000 rpm for 0.5 h) and washed with a 3 wt% HCl aqueous (500 mL) and DI water (2L), respectively, until the supernatant was colorless with a pH value around 6.5. In the end, the GO was collected and freeze dried for further use.

Chemical functionalization of GO

Functionalization with EDA or TETA

The prepared GO (200 mg) was initially dispersed in 200 Ml *N,N*-Dimethylformamide (DMF) and sonicated for 2.5 h, then, EDA (30 g) was added to the resulting GO suspension, followed by *N,N*-Dicyclohexylcarbodiimide (5 g) and sonication for 30 min. Subsequently, the resultant mixture was transferred to an oil bath (120 °C) and stirring for 48 h, after which, ethanol (60 mL) was added to the mixture obtained. After 12 h on standing, the supernatant liquid was removed, and the resulting bottom solid was filtrated with polytetrafluoroethylene membrane. Then, it was washed with ethanol (50 mL) and DI water (50 mL) to make sure the residue EDA was thoroughly removed, respectively. Finally, the final product was obtained by freeze-drying. TETA-GO was also prepared by the same procedure.

Functionalization with APTMS or APTES

The synthesized GO (200 mg) was taken in ethanol (150 mL) and loaded in a 250 mL round-bottom flask, followed by stirring and ultrasonicating the dispersion for 0.5 h. Subsequently, APTMS or APTES (369.6 mg, 2.0 mmol) was dropwise added into the suspension. The mixture was stirred and refluxed for 6 h. After cooling to room temperatures, the prepared APTMS-GO was filtrated and washed with absolute ethanol and water three times, respectively. A black solid was obtained after a freeze-drying procedure.

Fabrication of amine-GO/WPU nanocomposites

The preparation of amine-GO/WPU nanocomposites was carried out in a 250 mL three-necked, round-bottom flask equipped with a mechanical stirrer and condenser at a constant temperature oil bath, under a dry nitrogen atmosphere. First, 27 mg EDA-GO was dispersed and sonicated in 10 mL N-methyl-2-pyrrolidone (NMP) at room temperature for 3 h. Then, 0.005 mol Polybutyleneglycol adipate (PBA, number-average molecular weight of 2000) and 0.02 mol Isophorone diisocyanate (IPDI) were fed into the flask and reacted at 80 °C for 1 h. Additional chain extension reaction was carried out at the same temperature with 0.007 mol Dimethylolpropionic acid (DMPA) to form NCO terminated PU prepolymer for another 3 h. Afterward, the well-dispersed black suspension obtained at the first step above was mixed with prepolymer and vigorously stirred with the help of 0.05 g Dibutylbis (laurato) tin (DBTL, catalyst) at 80 for 1 h. The purpose of taking much higher amount of catalyst here was to make sure that the reaction between functionalized graphene nanoplatelets and PU chains can react more easily and durable. Subsequently, 0.007 mol Triethylamine (TEA) and 10 mL acetone were added under continuous stirring when the system was cooled to 50 °C. The former was used for reducing the system viscosity caused by the reaction between EDA-GO and prepolymer and the latter for neutralizing the carboxylic acid groups stemming from the DMPA monomer. After 45 min, the mixture was further cooled down to 10 °C, EDA (0.007 mol), being used for post-chain extension, dissolved in 42 mL of water was fed dropwise into the flask at 1800 rpm for 15 min to obtain an aqueous emulsion, followed by acetone-removing procedure. The resulting products were aqueous emulsions of EDA-GO/WPU nanocomposites with solid content of 28 wt%. For comparison, GO/WPU, TETA-GO/WPU, APTMS-GO/WPU, APTES-GO/WPU nanocomposites were also prepared following the same procedure. Finally, the films were prepared by casting the emulsion into Teflon plates and dried at 30 °C firstly in a convection oven for 12 h and then at 50 °C for 2 days.

Characterization

ATR-FTIR spectra of the functionalized graphene nanoplatelets were performed with a Nicolet 6700 infrared spectrometer using a DLaTGS detector. All spectra were carried out between 4000 and 500 cm^{-1} with averaging 32 scans at a resolution of 4 cm^{-1}. X-ray diffraction (XRD) patterns were recorded on an D8 X-ray diffractometer (Bruker AXS, German) at 40 kV and 40 mA using Cu Kα radiation ($\lambda = 1.5406$ Å), to identify the composition and phase of sample. The 2θ angle ranged from 3° to 50° at the scanning rate of 4 min^{-1}. Raman spectra were obtained on a confocal microscopic Raman spectrometer (Renishow In-Via, USA) with 532 nm laser light irradiation from 400 to 3000 cm^{-1} at a duration time of 10 s. Thermogravimetric analysis (TGA) was carried out using a Mettler TGA/SDTA 851 E analyzer in the temperature range of 25–700 °C at a heating rate of 10 and 20 °C min^{-1} for characterizing the graphene materials and nanocomposites, respectively. The samples were pressed into slices before analysis. Differential scanning calorimetry (DSC) analysis was carried out with a DSC 822e (Mettler Toledo, Columbus, Ohio, USA) in the temperature range of −80 to 200 °C under protection of N_2 with a flow of 50 mL^{-1}. X-ray photoelectron spectroscopy (XPS) analysis was conducted using an ESCALAB 250 Xi (Thermo, USA) X-ray photoelectron spectrometer with Al Kα line as the excitation source ($hv = 1484.6$ eV) to identify amine-GO samples. Transmission electron microscopy (TEM) and scanning electron microscopy (SEM) images including scanning electron microscope-energy dispersive spectrometer (SEM–EDS) were collected on a JEM-2100 (JEOL, Japan) transmission electron microscope at an accelerating voltage of 200 kV and an S-4800 (Hitachi, Japan) scanning electron microscope at an accelerating voltage of 3 kV to observe the morphologies of amine-GO and nanocomposites, respectively. Non-contact atomic force microscopy (AFM, Multimode 8, Brooke Technology Cop., Germany) was employed to determine the morphology and thicknesses of the exfoliated GO and amine-GO. The tensile properties of the nanocomposites were measured at room temperature by using an Instron 5565 universal testing machine (Illinois Tool Works Inc., Norwood, Massachusetts, USA). The dumbbell-shaped specimens with thickness of 0.5 mm, width of 2 mm, and length of 10 mm were prepared for the tensile tests. The crosshead speed was set at 50 mm min^{-1}. The tensile test results were measured as mean value of three specimens. The surface for hydrophobicity test and the surface roughness of nanocomposites were carried out on a DCA-315 contact angle measurement apparatus with ultrapure water as probe liquids at room temperature and observed with FESEM and AFM, respectively. Contact angles were measured at three different positions for one sample, and the results were expressed as mean value.

Results and discussion

Characterization of GO and amine-GO

FT-IR and TGA analyses of GO, and amine-GO

Figure 1a shows the FTIR spectra of GO and related amine-GO including EDA-GO, TETA-GO, APTES-GO, and APTMS-GO. The characteristic peaks located at 3400, 2927, 1720, 1636, and 1050 cm^{-1} in the GO spectra are ascribed to –OH, $–CH_2–$, C=O, and C–O bonds, respectively. As for amine-GO, a dramatic decrease in the intensity of the peak at 1720 cm^{-1} (C=O stretching in carboxylic acid), 1396 cm^{-1} (epoxide groups of the GO) is detected compared with pure GO, suggesting that GO have reacted with the modifiers. For EDA-GO and TETA-GO, the new characteristic band appeared at 1340 cm^{-1} corresponds to C–N stretching vibrations, suggesting the successfully functionalization of GO [27]. Furthermore, an increase in intensity of the peak at 1050 cm^{-1} is also detected after grafting organoamine on GO nanosheets. While for APTES-GO and APTMS-GO, the upcoming new bands at 1122, 1030, 776 and 690 cm^{-1} indicates the formation of Si–O–C, Si–O–Si, Si–H and Si–O–C, providing a strong evidence for the presence of silane on the GO platelets [28].

The results of the TGA of GO and amine-GO are shown in Fig. 1b. As can be seen, both of five TGA curves start to lose weight upon heating under N_2 atmosphere below 100 °C, due to the evaporation of water. As the temperature increases to 230 °C, GO is unstable and exhibits its major decomposition behavior (40 % weight loss) because of labile oxygen-containing functional moieties such as epoxy, hydroxyl, and carboxyl. While at the same temperature (230 °C), the weight loss of amine-GO

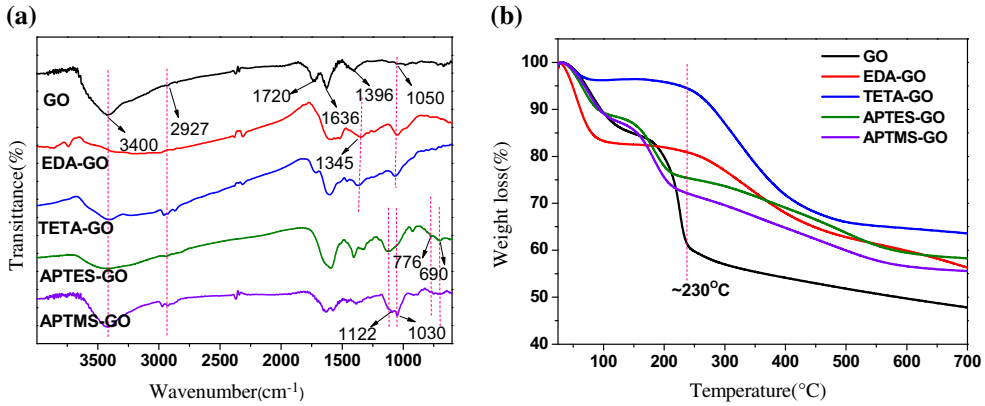

Figure 1 **a** FTIR spectra of GO, EDA-GO, TETA-GO, APTES-GO, and APTMS-GO. **b** TGA curves of GO, EDA-GO, TETA-GO, APTES-GO, and APTMS-GO.

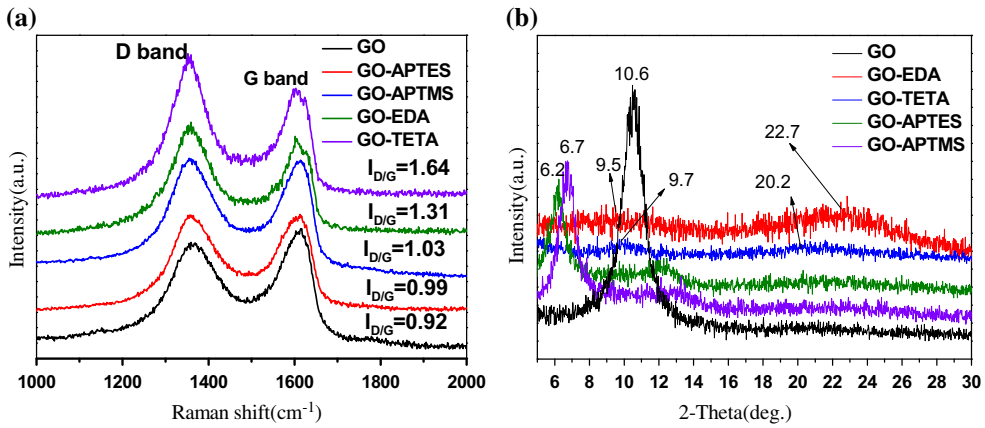

Figure 2 **a** Raman spectra of GO and amine-GO; **b** XRD patterns of GO and amine-GO.

nanoplatelets undergoes is 28 % of APTMS-GO, 25 % of APTES-GO, 20 % of EDA-GO, and 6 % of TETA-GO, respectively, which indicates that thermally labile O-containing functional groups are converted to other functional groups such as Si–O–Si/Si–O–C bands for APTES-GO (or APTMS-GO) or removed by EDA (or TETA) because of partially chemical reduction thereby resulting in much better thermal stability in comparison with GO [27, 28].

Raman and XRD analyses of GO, and amine-GO

Raman spectroscopy is one kind of powerful and most widely used technique to characterize the disorder and defect structure of graphene. As can be seen in Fig. 2a, graphene oxide shows two characteristic peaks generated at 1362, 1612 cm^{-1}, which are ascribed to D band (arises from the defects, edges effects, and disorder of carbon in graphene platelets) and G band (originates from the first-order scattering of the E_{2g} vibration mode and the in-plane vibration of ordered sp^2-bonded carbon atoms), respectively. After treatment with aminosilane-coupling agents, the intensity ratio (I_D/I_G) values (correspond to the amount of sp^3 hybridized carbon atoms in the sp^2 conjugated graphene) of amine-GO increase from 0.92 of GO to 0.99 of APTES-GO and 1.03 of APTMS-GO, which reveals a slightly increase in the amount of sp^3 hybridized carbon atoms resulted from the reduction of small sp^2 domains. Hence, we can reasonably suppose that the disorder domains and defect structures of graphene are slightly expanded by covalently bonding with APTES or APTMS [28]. While for EDA-GO and TETA-GO, the I_D/I_G intensity ratio value is found to increase up to 1.31 and 1.64, respectively. These results indicate the further distortion of bonds and extensive destruction of symmetry due to the reduction in size of in-plane sp^2 domains caused by the extra grafting with organoamine in comparison with GO in degree of the functionalization and structural imperfection. Moreover, the high degree of reduction and disorder on functionalized graphene

nanosheets implies that reacting sites located on GO platelets are attacked by our modifiers such as EDA and TETA. As a result, the new defects or edges that as a reflection on the increase in I_D/I_G ratio have provided direct evidence for our achievement in successfully functionalizing GO.

Figure 2b gives the XRD spectra of GO, EDA-GO, TETA-GO, and APTES-GO as well as APTMS-GO. It is well known that for the graphene oxide sample, the strong and sharp diffraction peak from (002) at $2\theta = 10.6°$ corresponds to the typical peak of layered GO. However, the (002) peaks of APTES-GO and APTMS-GO shifts from 10.6° to 6.2° and 6.7°, respectively, after GO being treated with APTES and APTMS. Correspondingly, the interlayer spacing undergoes an expansion from 0.83 to 1.41 and 1.31 nm, respectively. The resulting larger interlayer distance of these two sorts of GO can be attributed to the wrinkling or presence of functional groups between the interlayer structures caused by the successful intercalation of aminosilane-coupling agents [28]. While for GO functionalized with EDA and TETA, the peaks of resulting functionalized graphene nanosheets are weak and broad and appear at lower angles of 9.5° and 9.7°, respectively, and higher angles of 22.7° and 20.2°, respectively, the latter of which corresponds to d-spacings of 0.39 and 0.44 nm, respectively. This change can be attributed to the stitching of the exfoliated graphene nanoplatelets [27], confirming that EDA and TETA are adequately grafted on the graphene layers. These XRD results are well consistent with related Raman data.

TEM images, AFM images, and height profiles of GO and amine-GO

In order to measure the thickness of before and after treatment of GO materials, AFM observations are conducted. The ScanAsyst-mode AFM images of GO and amine-GO dispersed in ethanol are presented in Fig. 3. From the cross-sectional analysis, we could find the height of (A) GO, (C) TETA-GO, and (E) APTMS-GO, is 1.1, 0.8 and 2.5 nm, respectively, which corresponds well to the above XRD results that the interlayer spacing of TETA-GO and APTMS-GO is decreased and increased, respectively. Therefore, the change of amine-GO in thickness can be attributed to the presence of functionalized groups grafted on graphene sheets [27, 28]. Likewise, similar result has also been observed in the images of TEM which is employed to determine the morphology of graphene nanosheets. Figure 3b, d, f shows the morphology of GO, TETA-GO, and APTMS-GO, respectively. As can be observed from them, the whole parts of GO in Fig. 3b are obscure due to the overlapped sheets consist of 2–3 layers. Different from GO, the morphology of TETA-GO (Fig. 3d) presents a transparent and wrinkled nanoplatelet shape, which coincides much well with the results of XRD, AFM mentioned above. Such structure probably guarantees the thermodynamic stability for partially reduced and modified graphene by TETA. However, the TEM micrographs of APTMS-GO not only resembles the vivid (black) parts shown in TETA-GO but also retains the multiple layers kept by GO, which is substantially caused by the intercalation of APTMS. It again confirms that our APTMS is successfully covalent bonding with graphene.

XPS analyses of GO, APTMS-GO, and TETA-GO

X-ray photoelectron spectroscopic (XPS) measurements are performed for GO, APTMS-GO, and TETA-GO, and the results are presented in Fig. 4. Only C1s and O1s peaks are observed in the XPS survey spectrum of GO, but the N1s (399.5 eV) peaks appear in the XPS spectrum of both APTMS-GO and TETA-GO, while the Si2p (101.8 eV) peaks appear in the APTMS-GO. The high-resolution C1s spectra for GO, APTMS-GO, and TETA-GO are reproduced in Fig. 4b–d. Figure 4b shows four peaks at 284.8, 286.8, 287.8 and 288.6 eV, which represents the carbon bonds of C–C, C–O, C=O and O=C–C, respectively. Compared with GO, the C1s XPS spectra of APTMS-GO and TETA-GO shows a significantly decrease in the peak intensities of C–O and C, together with the appearance of C–Si peak (283.5 eV) [29] in Fig. 4c and C–N peak (285.7 eV) [27] in Fig. 4d. These results indicate that both of APTMS and TETA are successfully attached on the surfaces of graphene oxide via the reaction of silane groups, terminal amines with alkylcarboxyl groups in GO during the modification.

Characterization of nanocomposites

Dispersion, morphology of GO, and amine-GO in WPU matrix

Analyses of the fractured surfaces of neat WPU (A), GO/WPU (B) and amine-GO/WPU (C-D) in Fig. 5

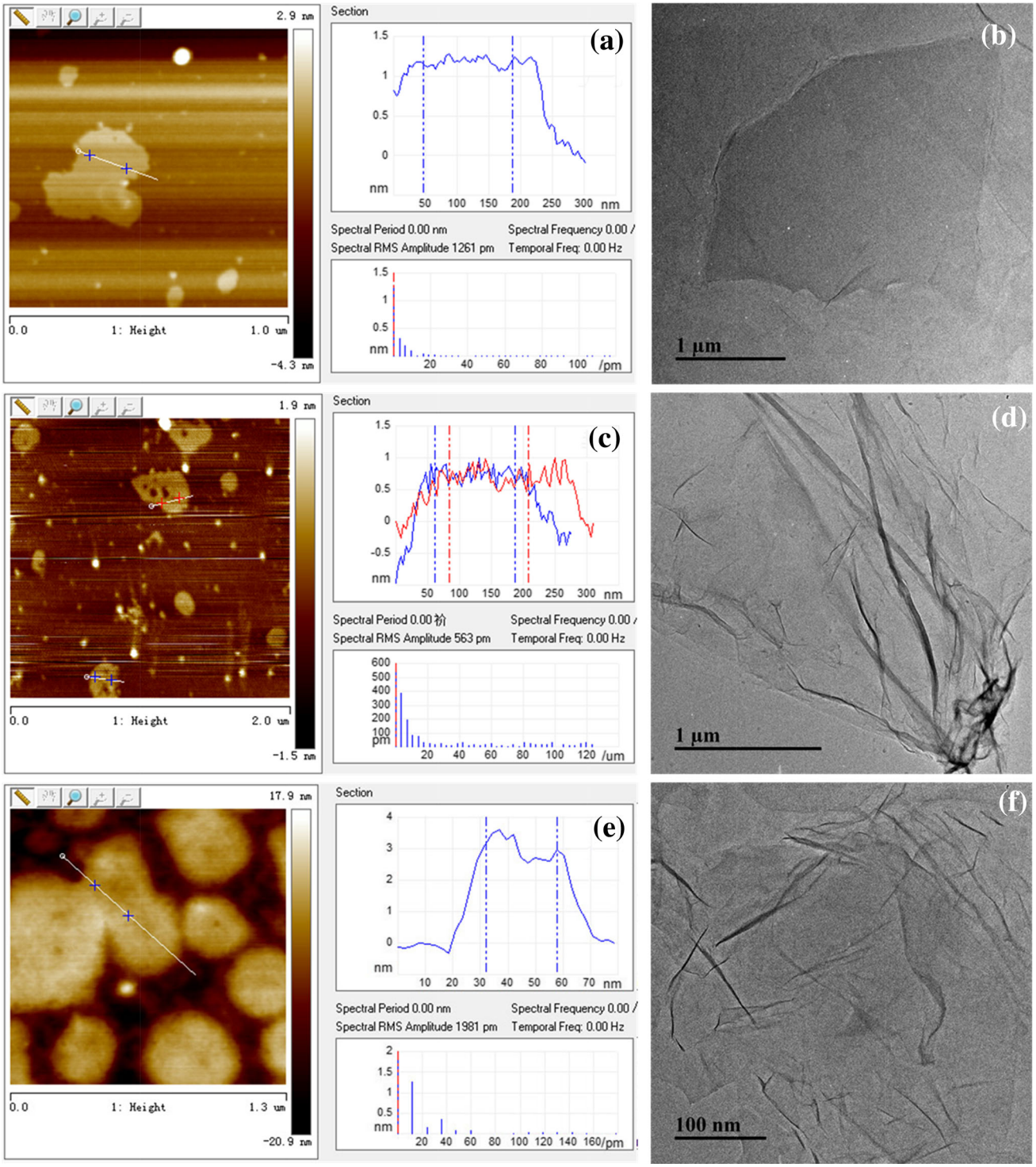

Figure 3 TEM images, AFM images, and height profiles of **a**, **b** GO; **c**, **d** TETA-GO; and **e**, **f** APTMS-GO.

discloses the microdispersion of inorganic nanofillers. In Fig. 5b, the untreated graphene oxide nanosheets are well dispersed in WPU matrix, due to the relatively strong hydrogen covalent interaction with the matrix. However, few agglomerates and some easy-to-aggregate nanoplatelets are observed on the fracture surface, which is caused by the fact that overlapped layers of GO cannot separate from

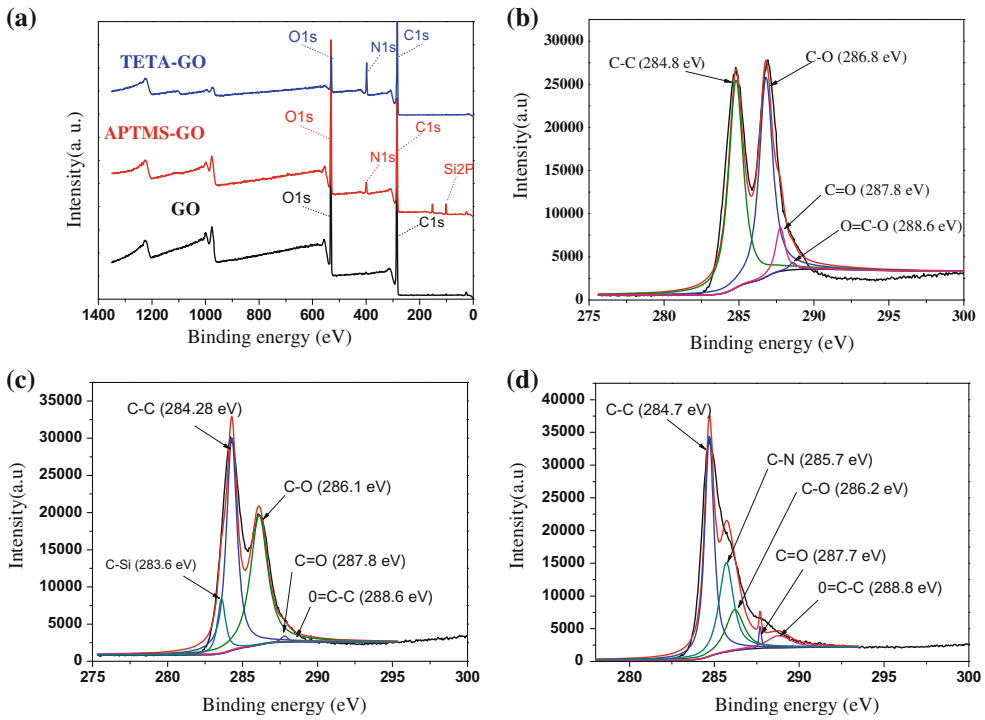

Figure 4 Full range XPS of spectra of GO, APTMS-GO, and TETA-GO (**a**). $C1_S$ XPS spectra of GO (**b**), APTMS-GO (**c**), and TETA-GO (**d**).

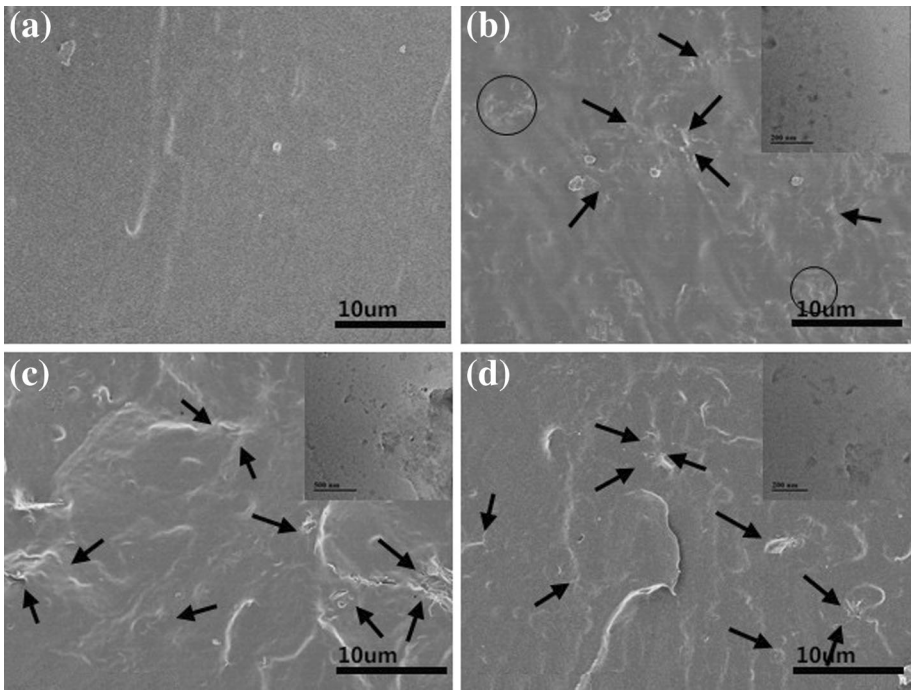

Figure 5 FE-SEM images of neat WPU (**a**), GO/WPU (**b**), TETA-GO/WPU, (**c**) and APTMS-GO/ (**d**). *Inset* photographs in (**b**–**d**) are TEM micrographs of GO/WPU, TETA-GO/WPU, and APTMS-GO/WPU, respectively. The *scale bars* for the *inset* TEM images are all 200 nm.

each other, thus tend to restack and attract. Whereas the amine-GO nanosheets in Fig. 5c, d are dispersed more uniformly and embedded deeper than GO in the WPU matrix, which can be explained by the strong interfacial covalent bonding between polymer and nanofillers [19]. Figure 5c, d reveals the difference between TETA-GO/WPU and APTMS-GO/WPU nanocomposites. The thickness and morphology of TETA-GO finely dispersed in WPU matrix shows small and paper-like, thereby achieving good compatibility and interfacial contact with the polymer. However, in the case of APTMS-GO, it partially projects outside from fracture surface of WPU indicating the better embedding and combining in the polymer matrix, which to a great extent can be reasoned by the mechanism that silane molecules are covalently attached on the GO surface by the hydrolysis of silane after functionalization. Meanwhile, their amino end-groups react with PU chains, resulting in the better embedding and dispersion of amine-GO in the matrix [20]. The inset TEM photographs of GO/WPU, TETA-GO/WPU, and APTMS-GO/WPU are shown in Fig. 5b–d, respectively, the dispersion of which agrees well with the FE-SEM images shown above.

Thermal properties

The (A) TGA and (B) DSC profiles for GO/WPU and amine-GO/WPU composites as a function of temperature are shown in Fig. 6. From the TGA curves, we can see that the incorporation of amine-GO including EDA-GO, TETA-GO, APTES-GO, and APTMS-GO can effectively enhance the thermal stability of WPU material. At loading of 0.15 wt% (the weight of amine-GO to the total weight of raw materials for preparing WPU before emulsifying) amine-GO or GO, the temperature of 10 % weight loss of amine-GO/WPU is 295 °C for EDA-GO/WPU, 291 °C for TETA-GO/WPU, 315 °C for APTMS-GO/WPU and 289 °C for APTES-GO/WPU, respectively, which shows a little big increase compared with 265 °C of pure WPU and 280 °C of GO/WPU. These results indicate that amine-GO/WPU composites have better thermal stability than pure WPU and can be explained by the reaction between $-NH_2$ grafted on graphene nanosheets and –NCO from PU chains, which in turn introduces the good heat resistance of graphene [19, 30]. Furthermore, the improvement in thermal stability can also be attributed to the so-called "tortuous path" effect of graphene platelets, which delays the escape of volatile degradation products and retards the diffusion of heat and mass transfer of products of pyrolysis [30]. Figure 6b shows the differential scanning calorimeter thermograms of the nanocomposites. The glass transition temperature (T_g) of GO/WPU and amine-GO/WPU nanocomposites shows almost no change compared with pure WPU. Such no difference in T_g is related primarily to the lower loading of amine-GO and can be explained by two aspects. First, the motion of soft-segment might be hindered by rigid graphene nanophase mediated by hydrogen bonding or chemical grafting onto active functionalized graphene platelets surface. It could result in the shift of T_g to high temperature. However, in the opposite way, incorporating amine-GO nanoplatelets might cleave the original interaction between hard- and soft-segments and hence change the microphase structure in WPU matrix, which will lead to the shift

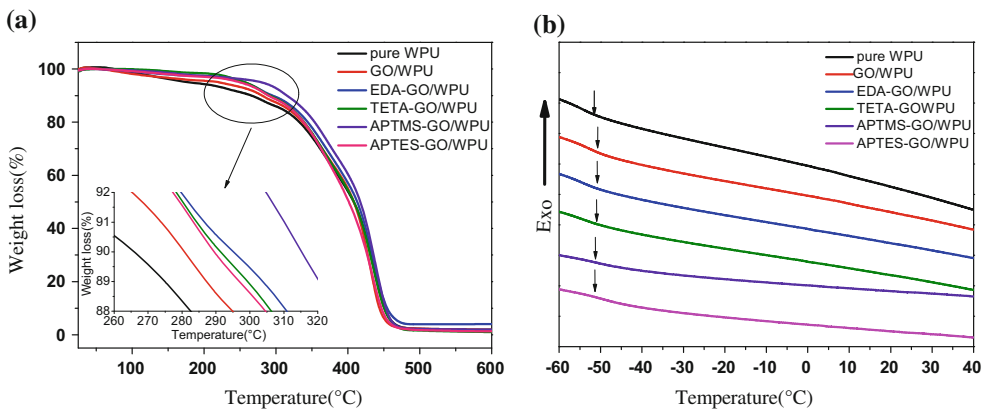

Figure 6 **a** TGA analyses of pure WPU and nanocomposites; **b** DSC thermograms of pure WPU and nanocomposites.

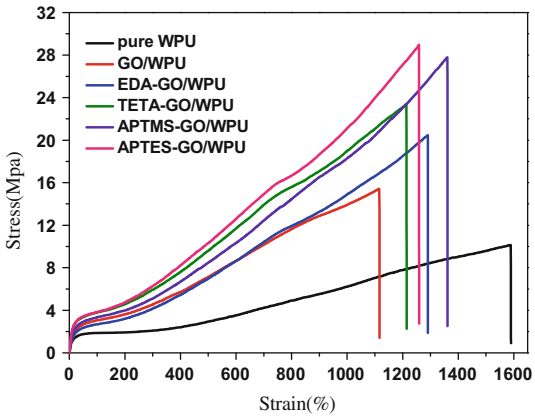

Figure 7 Stress–strain curves of pure WPU and nanocomposites.

of T_g to low temperature. Therefore, the change of nanocomposites in T_g compared with pure WPU is not obvious base on the above reciprocal inhibition mechanism [31].

Mechanical properties

The stress–strain curves of the pure WPU and composites are shown in Fig. 7. The tensile strength increases from 10.13 Mpa of the pure WPU film to 15.43, 20.43, 23.38, 27.79 and 28.96 Mpa for the GO/WPU, EDA-GO/WPU, TETA-GO/WPU, APTMS-GO/WPU, and APTES-GO/WPU, respectively. This result implies that the amine-GO/WPU composites have higher tensile strength than the pure WPU film and GO/WPU composite, in which the APTES-GO-treated composites show the largest increase in tensile strength. It indicates that the functional groups introduced by our modifiers play a vital role in increasing the interaction energy between inorganic nanomaterials and polymer matrix [17, 30, 32]. In addition, the increase in stress can be attributed to the well dispersion of amine-GO in polymer matrix, due to the strong hydrogen bond induced by the unpaired electrons on the amine group which in turn transfer the interfacial stress transfer, thereby serving as a dispersion aid for engineering interfacial compatibility and stability between amine-GO and the matrix. However, the elongation at break of four sorts of amine-GO/WPU films is decreased with the incorporation of 0.15 wt% amine-GO due to the reduction of elastic deformation. That can mainly be attributed to the fact that nanofillers will attract stress from the polymer and generate stress-focusing effect after the formation of the covalent bonding between the amine-GO and the PU polymer matrix, in addition, the rigid nanoplatelets cannot produce large elongation deformation, thus reducing the elastic deformation. In addition, it can be seen that the tensile stress of the APTMS-GO/WPU and APTES-GO/WPU is greater than that of EDA-GO/WPU and TETA-GO/WPU. This reveals that amine functional group on the aminosilane-coupling agents is more active than on the organoamine owing to the partially reduction reaction occurs on the surface of graphene modified by EDA or TETA. That can be confirmed by the EDS results (Fig. S1) that present the detailed elemental distributions of C, N, O, and Si, in which the percentage of element N incorporated in the matrix by aminosilane-coupling agents is higher than that of organoamine, verifying the more effective interfacial interaction between aminosilane-coupling agents and polymer, which coincides well with the analyses of XRD, AFM, and TEM.

Hydrophobicity behavior

Figure 8a shows contact angles of pure WPU and its nanocomposite films incorporated by GO, EDA-GO, TETA-GO, APTMS-GO, and APTES-GO, respectively. Contact angle values for WPU films were increased with the introduction of amine-GO and exhibited a slight increase from 70.3° of pure WPU to 82.65° of EDA-GO/WPU, 84.45° of TETA-GO/WPU, 86.2° of APTMS-GO/WPU, and 92.6° of APTES-GO/WPU, respectively, indicating that the hybrid WPU films form a hydrophobic surface. That can be ascribed to the partially reduction of EDA-GO and TETA-GO and the introduction of Siloxane (Si–O–Si) network structure originated from APTMS and APTES, removing the oxygen functionalities located on the basal plane of graphene oxide and introducing Si element into the structure of graphene nanosheets, respectively. Therefore, the hydrophobic of the films was improved to some extent by bringing the above hydrophobic substance such as platelets or Si element into the nanocomposites via in situ polymerization [33].

To further probe the enhancement in the hydrophobic of WPU films, FE-SEM and AFM are used to observe and analyze the surface roughness of amine-GO/WPU films. From the pictures of FE-SEM, we can see that pure WPU film is smooth (Fig. 8b), whereas the surface of amine-GO/WPU polymeric composite film in Fig. 8c, d clearly shows a structure

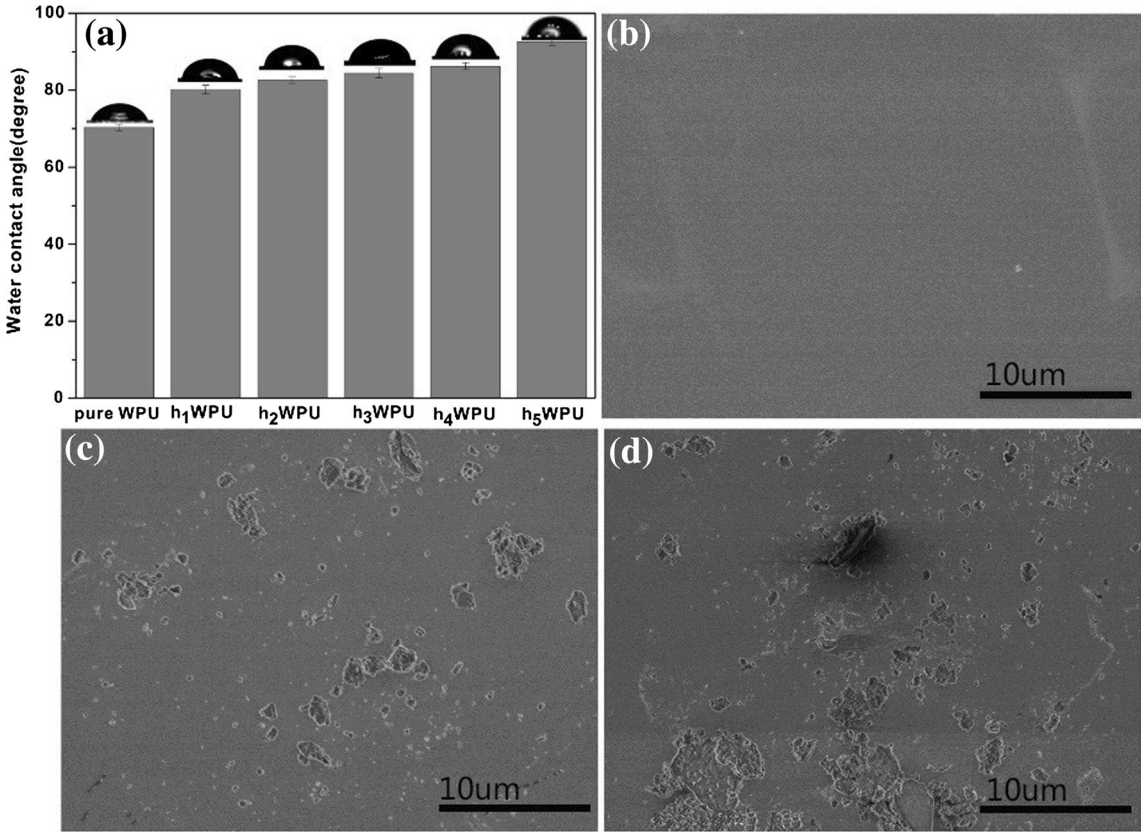

Figure 8 Contact angle of pure WPU and hybrid WPU (**a**), FE-SEM images of pure WPU (**b**), TETA-GO/WPU (**c**) and APTMS-GO/WPU (**d**) polymer films coated on silicon wafer. h_1–h_5WPU in **a** represents GO/WPU, EDA-GO/WPU, TETA-GO/WPU, APTMS-GO/WPU, and APTES-GO/WPU, respectively.

modified with layered amine-GO flakes that create a number of peaks and cavities thereby easily trapping large amount of air within them and making the liquid droplets to rest on a layer of air. While the results of AFM for analyzing the detail roughness are disclosed in supplementary information, we find that the value (Fig. S2) for the roughness of APTMS-GO/WPU is higher than that of TETA-GO/WPU and pure WPU, which keeps good agreement with the results of FE-SEM and hydrophobicity test.

Conclusions

In this article, the covalently functionalized graphene oxide nanosheets with two kinds of modifiers including organoamine- and aminosilane-coupling agents were successfully prepared and confirmed by FTIR, TGA, Raman, XRD, XPS, AFM and TEM. These amine-GO nanoplatelets were covalently incorporated into WPU matrix, forming EDA-GO/WPU, TETA-GO/WPU, APTMS-GO/WPU, and APTES-GO/WPU nanocomposites. SEM analyses and TEM images indicated that amine-GO nanosheets achieved homogenous dispersion in the matrix. The TGA analyses revealed that the amine-GO/WPU nanocomposites, especially the APTMS-GO/WPU, attained better thermal stability, with more than 24 °C higher than pure WPU and 9 °C higher than GO/WPU at 10 % weight loss. The glass transition temperature of amine-GO showed almost no change, compared with pure WPU. Owing to the homogenous dispersion in the matrix and the covalent bonding between the amine-GO and the polymer matrix, tensile strength was increased by 101–185 % and 132–187 %, compared with pure WPU and GO/WPU, respectively, in which APTES-GO/WPU achieved the largest increase. Additionally, the amine-GO/WPU composites also exhibited better hydrophobic behavior than the untreated WPU. These results indicated that the amine-GO exhibited great potential to yield high-performance graphene/WPU nanocomposite. In

addition, covalently functionalized graphene sheets with the silane-coupling agent will provide a more promising and better method to fabricate graphene-based polymer composites with effective reinforced performance than the organoamine, with all the properties above considered.

Acknowledgements

The authors gratefully acknowledge the financial supports from the Cooperative Innovation Foundation of Industry, Academy and Research Institutes (BY2013015-10, 2014023-08) in Jiangsu Province of China and the Fundamental Research Funds for the Central Universities (JUSRP51623A).

Electronic supplementary material: The online version of this article (doi:10.1007/s10853-016-9993-5) contains supplementary material, which is available to authorized users.

References

[1] Engels HW, Pirkl HG, Albers R et al (2013) Polyurethanes: versatile materials and sustainable problem solvers for today's challenges. Angew Chem Int Ed 52:9422–9441

[2] Wu G, Kong Z, Chen J et al (2014) Preparation and properties of waterborne polyurethane/epoxy resin composite coating from anionic terpene-based polyol dispersion. Prog Org Coat 77:315–321

[3] Elrebii M, Mabrouk AB, Boufi S (2014) Synthesis and properties of hybrid alkyd–acrylic dispersions and their use in VOC-free waterborne coatings. Prog Org Coat 77:757–764

[4] Wu Z, Wang H, Tian X et al (2014) Surface and mechanical properties of hydrophobic silica contained hybrid films of waterborne polyurethane and fluorinated polymethacrylate. Polymer 55:187–194

[5] Li SC, Wang LW, Wang JY (2012) Study on properties of modified nano-ZnO/WPU hybrid material. Adv Mater Res 510:742–746

[6] Ma XY, Zhang WD (2009) Effects of flower-like ZnO nanowhiskers on the mechanical, thermal and antibacterial properties of waterborne polyurethane. Polym Degrad Stab 94:1103–1109

[7] Kuan HC, Ma CCM, Chang WP et al (2005) Synthesis, thermal, mechanical and rheological properties of multiwall carbon nanotube/waterborne polyurethane nanocomposite. Compos Sci Technol 65:1703–1710

[8] Miklečić J, Blagojević SL, Petrič M et al (2015) Influence of TiO_2 and ZnO nanoparticles on properties of waterborne polyacrylate coating exposed to outdoor conditions. Prog Org Coat 89:67–74

[9] Awad S, Chen H, Chen G et al (2010) Free volumes, glass transitions, and cross-links in zinc oxide/waterborne polyurethane nanocomposites. Macromolecules 44:29–38

[10] Kim YJ, Kim BK (2014) Synthesis and properties of silanized waterborne polyurethane/graphene nanocomposites. Colloid Polym Sci 292:51–58

[11] Yang SY, Lin WN, Huang YL, Tien HW, Wang JY, Ma CCM, Li SM, Wang YS (2011) Synergetic effects of graphene platelets and carbon nanotubes on the mechanical and thermal properties of epoxy composites. Carbon 49:793–803

[12] Seyedin MZ, Razal JM, Innis PC et al (2015) Achieving outstanding mechanical performance in reinforced elastomeric composite fibers using large sheets of graphene oxide. Adv Funct Mater 25:94–104

[13] Li J, Ye F, Vaziri S et al (2013) Efficient inkjet printing of graphene. Adv Mater 25:3985–3992

[14] Balandin AA, Ghosh S, Bao W et al (2008) Superior thermal conductivity of single-layer graphene. Nano Lett 8:902–907

[15] Scheuermann GM, Rumi L, Steurer P et al (2009) Palladium nanoparticles on graphite oxide and its functionalized graphene derivatives as highly active catalysts for the Suzuki-Miyaura coupling reaction. J Am Chem Soc 131:8262–8270

[16] Bunch JS, Verbridge SS, Alden JS et al (2008) Impermeable atomic membranes from graphene sheets. Nano Lett 8:2458–2462

[17] Liang J, Huang Y, Zhang L et al (2009) Molecular-level dispersion of graphene into poly (vinyl alcohol) and effective reinforcement of their nanocomposites. Adv Funct Mater 19:2297–2302

[18] AngeláRodriguez-Perez M, de Saja JA, AngeláLopez-Manchado M (2008) Functionalized graphene sheet filled silicone foam nanocomposites. J Mater Chem 18:2221–2226

[19] Wang X, Hu Y, Song L et al (2011) In situ polymerization of graphene nanosheets and polyurethane with enhanced mechanical and thermal properties. J Mater Chem 21:4222–4227

[20] Wang X, Xing W, Song L et al (2012) Fabrication and characterization of graphene-reinforced waterborne polyurethane nanocomposite coatings by the sol–gel method. Surf Coat Technol 206:4778–4784

[21] Appel AK, Thomann R, Mülhaupt R (2012) Polyurethane nanocomposites prepared from solvent-free stable dispersions of functionalized graphene nanosheets in polyols. Polymer 53:4931–4939

[22] Qian X, Song L, Yu B et al (2014) One-pot surface functionalization and reduction of graphene oxide with long-

chain molecules: preparation and its enhancement on the thermal and mechanical properties of polyurea. Chem Eng J 236:233–241

[23] Han S, Chun BC (2014) Preparation of polyurethane nanocomposites via covalent incorporation of functionalized graphene and its shape memory effect. Compos A Appl Sci Manuf 58:65–72

[24] Li X, Cheng Y, Zhang H et al (2015) Efficient CO_2 capture by functionalized graphene oxide nanosheets as fillers to fabricate multi-permselective mixed matrix membranes. ACS Appl Mater Interfaces 7:5528–5537

[25] Liu F, Wu L, Song Y et al (2015) Effect of molecular chain length on the properties of amine-functionalized graphene oxide nanosheets/epoxy resins nanocomposites. RSC Adv 5:45987–45995

[26] Du J, Lai X, Yang N et al (2010) Hierarchically ordered macro–mesoporous TiO_2–graphene composite films: improved mass transfer, reduced charge recombination, and their enhanced photocatalytic activities. ACS Nano 5:590–596

[27] Kim NH, Kuila T, Lee JH (2013) Simultaneous reduction, functionalization and stitching of graphene oxide with ethylenediamine for composites application. J Mater Chem A 1:1349–1358

[28] Matsuo Y, Nishino Y, Fukutsuka T et al (2007) Introduction of amino groups into the interlayer space of graphite oxide using 3-aminopropylethoxysilanes. Carbon 45:1384–1390

[29] Yang H, Li F, Shan C et al (2009) Covalent functionalization of chemically converted graphene sheets via silane and its reinforcement. J Mater Chem 19:4632–4638

[30] Yadav SK, Cho JW (2013) Functionalized graphene nanoplatelets for enhanced mechanical and thermal properties of polyurethane nanocomposites. Appl Surf Sci 266:360–367

[31] Liao K-H, Aoyama S, Abdala AA et al (2014) Does graphene change Tg of nanocomposites? Macromolecules 47:8311–8319

[32] Cao Y, Feng J, Wu P (2010) Preparation of organically dispersible graphene nanosheet powders through a lyophilization method and their poly (lactic acid) composites. Carbon 48:3834–3839

[33] Bharathidasan T, Narayanan TN, Sathyanaryanan S et al (2015) Above 170° water contact angle and oleophobicity of fluorinated graphene oxide based transparent polymeric films. Carbon 84:207–213